Cancer Letters 637 (2026) 218128

Contents lists available at ScienceDirect

Cancer Letters

journal homepage: www.elsevier.com/locate/canlet

Original Articles

Nanoformulation of a Pin1 inhibitor potentiates the efficacy of liposomal doxorubicin in second-line therapy for ovarian cancer

Gloria Saorin [a,1], Matteo Mauceri [a,1], Isabella Caligiuri [b,*], Urska Kamensek [c], Simona Kranjc Brezar [c], Giuseppe Corona [d], Ombretta Repetto [d], Tiziana Perin [b], Gabriele Grassi [e], Carlotta Granchi [f], Tiziano Tuccinardi [f], Maja Cemazar [c], Vincenzo Canzonieri [b,g], Muhammad Adeel [a], Flavio Rizzolio [a,b,**]

[a] Department of Molecular Sciences and Nanosystems, Ca' Foscari University of Venice, 30172, Venice, Italy
[b] Pathology Unit, Centro di Riferimento Oncologico di Aviano (C.R.O.) IRCCS, 33081, Aviano, Italy
[c] Department of Experimental Oncology, Institute of Oncology Ljubljana, Zaloska cesta 5, SI-1000, Ljubljana, Slovenia
[d] Immunopathology and Cancer Biomarkers, Centro di Riferimento Oncologico di Aviano (C.R.O.) IRCCS, 33081, Aviano, Italy
[e] Clinical Department of Medical, Surgical and Health Sciences, Cattinara University Hospital, Trieste Univer-sity, Trieste, Italy
[f] Department of Pharmacy, University of Pisa, 56124, Pisa, Italy
[g] Department of Medical, Surgical and Health Sciences, University of Trieste, 34149, Trieste, Italy

ARTICLE INFO

Keywords:
Nanocrystals
Drug delivery systems
Drug synergism

ABSTRACT

The second-line therapy for high-grade serous ovarian cancer (HGSOC) patients is generally ineffective. Drug selection is not aimed at improving overall survival, but rather based on residual toxicities, clinical judgment, and patient adherence. Therefore, the identification of more effective and targeted therapeutic strategies is critically needed. The Peptidyl-prolyl cis-trans isomerase NIMA-interacting 1 (PIN1) has emerged as a key hallmark of cancer progression and represents a promising therapeutic target in ovarian cancer (OC). VS10, a novel PIN1 inhibitor developed by our group, has shown potent activity against ovarian cancer cell lines.

In this study, a drug delivery system for VS10 was developed by formulating the inhibitor into nanocrystals stabilized with human serum albumin. Comprehensive physicochemical characterization of the formulation was performed using spectrophotometric quantification, dynamic light scattering (DLS) with zeta potential analysis, transmission electron microscopy (TEM), X-ray diffraction (XRD), fourier-transform infrared spectroscopy (FT-IR), and nuclear magnetic resonance (NMR). The nanocrystals exhibited favorable sustained release kinetics, as confirmed by in vitro release tests.

The anticancer activity was further validated through IC_{50} determinations on OC cell lines, and the therapeutic potential was assessed in vivo using an OC xenograft model. The VS10-loaded nanocrystals significantly inhibited tumor growth, and histopathological analysis confirmed the absence of systemic toxicity. Notably, co-administration with pegylated liposomal doxorubicin, a clinically approved chemotherapeutic agent, produced a synergistic effect, further enhancing tumor suppression. These findings support the potential of VS10, delivered via albumin-stabilized nanocrystals, as a promising second line therapy for OC.

1. Introduction

Cancer is the second cause of death in the world, overcome only by cardiovascular diseases [1]. OC is the main gynaecological cancer and the fifth cause of death for women [2]. The high mortality rate of OC is related to the late diagnosis since patients reveal clear symptoms mainly at metastatic stage. Indeed, if diagnosed at stage I, OC has a survival rate of 92.4 %, however the 63 % of OCs are diagnosed at stage IV dramatically reducing the life expectancy (27.6 % five years survival rate) [3]. The term OC comprises more than 30 types of cancer but the majority of

* Corresponding author. Pathology Unit, Centro di Riferimento Oncologico di Aviano (C.R.O.) IRCCS, 33081, Aviano, Italy.
** Corresponding author. Department of Molecular Sciences and Nanosystems, Ca' Foscari University of Venice, 30172, Venice, Italy
E-mail addresses: isabella.caligiuri@cro.it (I. Caligiuri), flavio.rizzolio@unive.it (F. Rizzolio).
[1] Authors contributed equally.

https://doi.org/10.1016/j.canlet.2025.218128
Received 8 June 2025; Received in revised form 15 October 2025; Accepted 8 November 2025
Available online 13 November 2025
0304-3835/© 2025 The Authors. Published by Elsevier B.V. This is an open access article under the CC BY-NC-ND license (http://creativecommons.org/licenses/by-nc-nd/4.0/).

them (almost 90 %) are epithelial OC, among which the most common is the serous subtype, which occurs in 70–80 % of cases as high grade tumors [4,5]. Currently, the standard treatment for OC comprises surgery, when possible, and platinum-based chemotherapy. Relapses are common and when occur, second line chemotherapies are applied. Unfortunately, recurrent OC has a discouraging prognosis and second line therapies are selected not in term of efficacy but dependent upon residual toxicities, physician preference, and patient convenience [6]. To overcome this issue, and improve patient survival, researchers are exploring the molecular networks of cancer cells to individuate new target therapies [7–9]. In this context, PIN1 protein is attracting a growing interest, started from its activity in controlling key proteins of the cell cycle process, an important hallmark of cancer development [10]. In addition to cell cycle proteins, numerous targets associated with various hallmarks of cancer rely on their phosphorylation status, regulated by protein kinases and phosphatases. Pin1, with its distinctive function of catalyzing the isomerization of the peptide bond between phosphorylated serine/threonine followed by proline, plays an essential role in these biological activities [11]. Proline isomerization, facilitated by Pin1, leads to modifications in the protein 3D conformation, stability, protein-protein interactions, localization, and other sites of phosphorylation/dephosphorylation. These alterations, in turn, impact the cellular functions of the target proteins [11]. In cancer cells, PIN1 works as a putative oncogene on different hallmark cancer proteins, including cyclin D1 [12], retinoblastoma protein [13,14], beta-catenin [15] p53 [16], c-myc [17] and FoxO3 [18]. Among cancer types, it is important in hormone sensitive cancers [19–22] including OC as demonstrated by our group [13,21,23]. The significant role of Pin1 in cancer, makes it a promising target for therapy. Indeed, PIN1-knokout mice proved to hamper the action of important oncogenes, such as Neu and Ras from inducing breast tumors [24]. Tissue specific Pin1 overexpression in mice induces centrosome overamplifications and eventually malignant mammary tumors formation during aging [25]. However, Pin1-knokout mice develop normally without gross abnormality (reduced side effects from drug inhibitors) although some age-dependent phenotypes such as neurodegeneration, retinal and testicular atrophy were described [26].

Pin1 activities are mainly due to two domains: PPIase and WW (two conserved tryptopans) connected by a flexible linker. The recognition of the substrate was reported for both domains while the PPIase is the only catalytic site [27]. Both domains can be targeted to inhibit PIN1, and indeed, different inhibitors were developed, even though most of them target the catalytic domain. The first developed inhibitor was Juglone (1998), which irreversibly inhibits the PPIase domain activity (10–20 μM) and was proved to inhibit the PIN1 protein expression in cells. Juglone activity over different cancers, among which, prostate, glioblastoma, hepatocellular and lung carcinoma was proved [28–33]. However, the in vivo use of Juglone was affected by its lack in selectivity with off-target related problems. After Juglone development, many other inhibitors were studied trying to overcome the selectivity issue and still nowadays efforts are made to develop Pin1 inhibitors suitable for in vivo applications. The FDA approved drug, all-trans retinoic acid (ATRA), for acute promyelocytic leukemia was identified as PIN1 inhibitor by binding the PPIase domain. ATRA was proved to cause PIN1 downregulation and degradation and was deeply studied in vivo [34]. Since ATRA have a short half-life in vivo, a slow-release formulation of the drug was studied demonstrating to being active over hepatocellular and breast cancer xenograft mouse models [34,35]. ATRA has been found to synergize with both sorafenib, a multi-kinase inhibitor used in hepatocellular cancer treatment [36], and arsenic trioxide (ATO), for the treatment of breast cancer [37,38]. ATO binds PPIase domain thought noncovalent interaction bringing to Pin1 degradation [37]. While ATRA remains of pharmacological interest, its mechanism of action involves direct binding to retinoic acid nuclear receptors, and it cannot be considered as a specific Pin1 inhibitor. By screening a drug library, a potent selective Pin1 inhibitor called KPT-6566 was identified and then proved to exert anticancer activity over breast, prostate, lung, and pancreatic cancers. This molecule not only inhibit Pin1 activity but also induce cell death by ROS production [39]. Similarly, to the identification of KPT-6566, our group, by a consensus docking approach, identified a powerful Pin1 inhibitor called VS10 [40]. VS10 was proved to be active over OC cell lines, provoking the proteasomal degradation of Pin1 together with the reduction of the levels of downstream targets β-catenin, cyclin D1, and pSer473-Akt.

Since drug delivery systems (DDS) could ameliorate the biodistribution and therefore the selectivity of drugs, a few groups started to design smarter deliveries of Pin1 inhibitors. Our group successfully encapsulated a Pin1 inhibitor developed by Guo et al., 2014, called compound n°17 (C17), into liposomes [23,41]. C17 showed Pin1 excellent inhibitory potency over the enzyme but very low antiproliferative activity on cancer cells, but this limitation was overcome by the liposomal formulation that allowed to prove its activity against OC in vivo. Recently our group produced a new, easy obtaining, polymeric formulation of C17 that confirmed the previously reported activity of the liposomal formulation [42].

Although, the activity of C17 can be recovered by its encapsulation into DDS, we decided to further study the encapsulation of VS10, which was already proved to be a promising antiproliferative drug for OC. Furthermore, VS10 is slightly soluble and its powder showed a crystalline structure, making it a good candidate for the development of nanocrystals. Nanocrystals represent intelligent DDS, as they enable the formulation of poorly soluble drugs into stable aqueous dispersions with enhanced drug content [43]. Furthermore, nanocrystals are DDS mainly constituted by the drug itself, indeed no matrices are used for encapsulation, but only ligands to stabilize their surface, allowing to avoid issues related to matrix elimination from the body. Nanocrystals reported in this work were produced by the aid of surfactants, but after their production, nanocrystals coating was exchanged with human serum albumin obtaining an increased biocompatibility and possibly facilitate drug intake from cells [44–47]. Beside the proof of in vivo activity of VS10 and its DDS over OC, more importantly, in this work the synergism between the Pin1 inhibitor and doxorubicin was assessed. This synergism was studied both in vitro and in vivo, by using the pegylated liposomal doxorubicin (PLDoxo), i.e. the inhibitor allows to ameliorate the second line treatment for OC and so being a promising new treatment for this kind of cancer, which unfortunately still has poor prognosis for most of the patients.

2. Materials and methods

2.1. Materials

The following materials were purchased: Pluronic® F-127 powder (suitable for cell culture, Cat. No. P2443), hexadecyltrimethylammonium bromide (CTAB, ≥98 %, Cat. No. H5882), human serum albumin (HSA, ≥96 %, Cat. No. A3782), Deuterated dimethyl sulfoxide (d-DMSO) (Cat. No. 151874), Dulbecco's Phosphate Buffered Saline (DPBS, Cat. No. D1408), and RPMI 1640 Medium with GlutaMAX™ Supplement (Cat. No. 61870044) from Merck, Darmstadt, Germany. Methanol for LC/MS (Cat. No. A177150010) was obtained from Carlo Erba, Milan, Italy, and chloroform (Cat. No. 67-66-3) from Thermo Fisher Scientific, Waltham, MA, US. Water was purified using a Milli-Q® (Millipak® 0.22 μm) system. Matrigel® Matrix High Concentration (HC, Cat. No. 354262) was sourced from Corning. The VS10 compound was produced by Enamine, Kiev, Ukraine. Bradford dye reagent (Cat. No. 500–0006) was procured from Bio-Rad, Hercules, CA, USA. Doxorubicin and PLDoxo were supplied by the National Cancer Institute pharmacy. OVCAR5, SK-OV-3, and KURAMOCHI cell lines, representing OC, were generously provided by Dr. Gustavo Baldassarre at the National Cancer Institute CRO-Aviano.

2.2. Methods

2.2.1. Nanocrystallization protocol

For the aqueous dispersion of nanocrystals, we processed VS10 powder according to the protocol outlined by Ref. [48]. Initially, a thin film was created by drying a mixture of 24 mg of F127 and 6 mg of VS10 dissolved in 3 mL of chloroform using a rotary evaporator. The thin film was then hydrated with 6 mL of MQ water and sonicated using a bath sonicator for 1 min, followed by probe sonication for 10 min at 40 % frequency in ice. This procedure yielded a VS10 nanocrystal dispersion stabilized by F127, referred to as VS10-F. Repeating the protocol with 2.4 mg of CTAB instead of F127 resulted in VS10-C, a CTAB-stabilized nanocrystal dispersion.

To replace surfactants with HSA, VS10-F and VS10-C were mixed with 4 mg/mL HSA under rotation at 30 rpm at room temperature for 24 h. The mixtures were then centrifuged twice (38,000 rpm, 4 °C, 1 h). The resulting pellet was lyophilized and redispersed in the original volume of MQ water using Sonics & Materials VC50 (Newtown, Connecticut, USA) probe sonicator (10 min, 40 % frequency). This stabilizers exchange process produced VS10-AF and VS10-CF from VS10-F and VS10-C, respectively.

2.2.2. Spectrophotometric quantifications

VS10 concentrations were quantified using a Cary 100 Agilent UV–VIS spectrophotometer (Santa Clara, California, USA) through a calibration curve method, measuring absorbance at 300 nm. VS10-F and VS10-C samples were diluted in methanol and directly measured. For VS10-AF and VS10-CF, methanol dilutions were centrifuged (2 min, 10,000 rpm) before analysis. HSA concentrations were quantified using a Bradford assay, measuring absorbance at 595 nm.

The yield percentage of the nanocrystal dispersions was calculated using the formula:

$$yield\ \% = \frac{C_{measured}[VS10]}{C_{theoretical}[VS10]} * 100$$

2.2.3. VS10 chemico-physical characteristics

The VS10 molecule characteristics were in silico predicted by Chemicalize software (Chemicalize.com; ChemAxon Ltd., Budapest, Hungary) and ALOGPS 2.1 software. Water solubility was also experimentally determined by dissolving 1 mg/ml of VS10 in MQ water, mixed 1 h and centrifuged 10000 rpm for 20 min. The supernatant was then analyzed for quantifying VS10 as reported for VS10-C and VS10-F.

2.2.4. Transmission electron microscopy (TEM)

A drop of solution (about 25 μL) was deposited on a 400-mesh holey film grid; after staining with 1 % uranyl acetate (2 min), the sample was observed with a FEI Tecnai G2 transmission electron microscope operating at 100 kV (Hillsboro, Oregon, US). The images were taken with a Veleta digital camera (Olympus Soft Imaging System). Image processing to outline crystals was carried out by ImageJ (1.52a) software.

2.2.5. Dynamic light scattering (DLS) and Z potential

Nanocrystals polidispersity and Z potential were analyzed by Zetasizer Nano particle analyzer (Malvern Panalytical, Malvern, UK). *2.2.4*.

2.2.6. X-ray diffraction (XRD)

X-ray diffraction analysis was conducted to characterize the crystalline structure of the nanocrystals. After an additional centrifugation step (1 h at 4 °C and 38,000 rpm), the nanocrystal pellets were lyophilized. The lyophilized powders were then analyzed using a Philips X-ray diffractometer equipped with a PW1050/70 goniometer, employing CuKα radiation (λ = 1.54178 Å). The diffractograms were obtained with an intensity detection step of 0.05° and were normalized for comparison, considering the signal-to-noise ratio influenced by the sample quantity.

2.2.7. Fourier-transform infrared (FT-IR) spectroscopy

FT-IR spectroscopy was performed on the cleaned and lyophilized nanocrystals to ascertain their molecular structure. KBr disks were prepared using the powder samples, and their FTIR spectra were recorded using a Perkin Elmer-Spectrum One spectrophotometer.

2.2.8. Proton nuclear magnetic resonance

VS10 powder and pellet of as previously reported cleaned VS10-F were dissolved in d-DMSO. Spectra were acquired by Bruker 400 MHz Advance spectrometer (Bruker, Billerica, Massachusetts). Acquisition parameters consisted in a 20.02 ppm spectral width, 30° pulse, 4.08 s acquisition time, 1s relaxation delay, 64000 data points, 64 scans. MestReNova® (Mestrelab Research, Santiago de Compostela, Spagna) software was used to analyze the results.

2.2.9. Release test

The release kinetics of VS10 from the nanocrystals were assessed using a dialysis method. 1 mL of VS10-F was enclosed in a Slide-A-Lyzer MINI Dialysis Device (20 k MWCO, Thermo Scientific, MA, USA) and dialyzed against DPBS at 37 °C. Aliquots were collected from inside the device at predetermined intervals and analyzed for VS10 content using UV–VIS spectrometry. The release percentage was calculated using the formula:

$$Release\ \% = 100 * \frac{[VS10]_{t0} - [VS10]_{tx}}{[VS10]_{t0}}$$

With $[VS10]_{t0}$ represents the initial concentration of VS10 in the sample, and $[VS10]_{tx}$ is the concentration at various time points.

2.2.10. IC50, drug combination tests and caspase 3/7 assay

The half-maximal inhibitory concentration (IC_{50}) of the drugs was determined on OC cell lines (OVCAR5, KURAMOCHI, and SK-OV-3). Cells were seeded at 1.5 x 10^3 cells/well in 96-well plates and treated the next day with 1:10 serial dilutions of the drugs, using cisplatin as a control (n = 3 independent experiments, each performed in triplicate).

Drug combination efficacy was evaluated on the same cell lines. Cells were exposed to 1:2 serial dilutions of Doxorubicin, PLDoxo, ATRA, VS10, and VS10AF, and combinations thereof. Starting concentrations were set at 25 μM for Doxorubicin, 50 μM for PLDoxo, 200 μM for ATRA, VS10, and VS10AF. Cell viability was measured using CellTiter-Glo (Promega, G7571) and read with a BioTek Synergy H1 plate reader. IC50 values were computed using GraphPad Prism, and drug interactions were analyzed using the Bliss independence model [49]. Expected mortality for drug combinations was calculated using the Bliss independence model, according to the formula:

$$E = A + B - (A * B)$$

where *A* and B represent the mortality induced by single-agent treatments.

Caspase 3/7 assay: SK-OV-3 cells (1.5 x 10^3 cells/well) were seeded in 96-well plates and treated the following day with PLDoxo (12.5, 6.25, 3.13 μM), VS10 (50, 25, 12.5 μM), and their combinations. Untreated cells were used as negative control, while cisplatin (10 μM) was included as positive control. Caspase activity was assessed at 6, 48 and 72 h post-treatment using the Caspase-Glo® 3/7 Assay (Promega, cat. G8090) and analyze with a BioTek Synergy H1 plate reader. Data were normalized to the luminescence of untreated controls.

2.2.11. Phospho-Histone H2A.X (Ser139) immunofluorescence assay

SK-OV-3 cells were seeded at a density of 2 × 10^4 cells per well in 8-well chamber slides (Thermo Scientific). After 24 h, cells were treated with PLDoxo (12.5 μM and 6.25 μM), VS10 (50 μM and 25 μM), and their combinations. Untreated cells were used as negative control, and cisplatin (10 μM) was included as positive control. At each time point (6, 24, and 48 h), cells were washed twice with DPBS (cat. 14190169,

Gibco, Waltham, Massachusetts, USA) and fixed for 20 min with 4 % paraformaldehyde. After fixation, cells were washed twice with DPBS and permeabilized with 0.3 % Triton-X100 in DPBS for 15 min. Following three washes, samples were incubated overnight at 4 °C with the primary antibody anti-phospho-Histone H2A.X (Ser139) (cat. 9718, Cell Signaling, Danvers, Massachusetts, USA) (1:100, 1 % BSA in DPBS). The following day, cells were washed twice and incubated for 1 h at room temperature in the dark with Goat anti-Rabbit IgG Alexa Fluor™ Plus 488 secondary antibody (cat. A32731, Invitrogen, Waltham, Massachusetts, USA) (1:1000, 1 % BSA in DPBS). After washing, nuclei were counterstained with DAPI (0.1 μg/mL in DPBS), and coverslips were mounted using a fluorescence mounting medium. Images were acquired using a Nikon Eclipse Ti2 equipped with an X-Light V2 L-FOV spinning disk confocal system. Images were analyzed using ImageJ to quantify the γH2A.X signal, and the mean ± standard deviation were calculated from three independent experiments.

2.2.12. Tumor growth analyses

Tumor growth was studied under the approval and guidance of the National Ethical Committee and the Administration of the Republic of Slovenia for Food Safety, Veterinary and Plant Protection. 5 x 10^3 OVCAR5 cells, suspended in 100 μL of a PBS and 30 % Matrigel/HC mixture, were subcutaneously implanted into the flanks of 6-week-old female athymic nude FOXN1NU mice. The treatment was done intraperitoneally once tumors reached an average size of 34 ± 11 mm^3. The treatment regimen included thrice-weekly doses of VS10AF (12.5 mg/kg, intraperitoneally) and PLDoxo (1.5 mg/kg, intravenously), as well as their combination for four weeks. To determine the therapeutic efficacy, tumors were measured every 2–3 days using a digital caliper in three perpendicular directions (a, b, c). Tumor volume was calculated using the following formula: V = a × b × c × π/6. Interpolation of unknown volumes was obtained using the following formula:

$$V_X = V_L + \frac{((V_R - V_L)*t_{gap})}{t_2 - t_1}$$

where V_X represents the unknown volume, V_L and V_R respectively indicate the volume measurements along the y-axis and x-axis. t_{gap} is the sequential number of days during which no measurements were taken, t_1 is the day of the last measurement obtained before the gap period, and t_2 is the day of the first measurement obtained after the gap period.

Tumor growth and mouse weight curves were plotted for each individual mouse and for the group average. The arithmetic means (AM) for each group were calculated from the tumor volumes, and the tumor growth curves were plotted with error bars representing the standard error of the mean (SEM).

2.2.13. Histopathology analyses

For histopathological evaluation, collected tissues were fixed in 10 % phosphate-buffered formalin and subsequently embedded in paraffin. Five-micrometer sections were prepared and stained with hematoxylin and eosin (H&E). These sections were then examined by pathologists for signs of toxicity or any other histopathological changes.

3. Results and discussion

3.1. Chemico-physical characteristics

VS10 i.e. the name attributed to 3-(3-methylbenzofuran-2-carboxamido)-5-phenylthiophene-2-carboxylic acid is a lipophilic, very slightly soluble, compound. VS10 solubility and polarity are influenced by pH since the molecule contains two acid groups. The carboxyl and the amide one with pKa of 3.56 and 13.73, respectively. These groups generate three possible microspecies (Fig. 1A). i.e. at the increment of pH, the neutral subside in favor of the monoanionic and then to the double anionic. These charges increase hydrophilicity and solubility (Fig. 1B) but only for extremely basic pH, not suitable for biological environment. Indeed, VS10 solubility at neutral pH, determined by Chemicalize software, is equal to about 114 μg/ml. This value was confirmed by experimental data with a solubility of 190 ± 30 μg/ml in MQ water.

3.2. Nanocrystals dispersions analysis

As can be appreciated in Fig. 1C, through the nanocrystallization protocol a VS10 concentration up to 800 ± 20 μg/ml can be obtained, i.e. an aqueous dispersion with a drug content four times as much its solubility in MQ water. HSA quantification proved the successful stabilizers exchange.

3.3. Nanocrystals characterization

As reported by Park et al. [48], surfactants that can be used to successfully stabilize nanocrystals are CTAB and F127. In the case of VS10, we decided to test the effects of both polymers in order to evaluate differences in chemical-physical parameters of the obtained nanocrystals. As previously reported for nanocrystals of monoacylglycerol

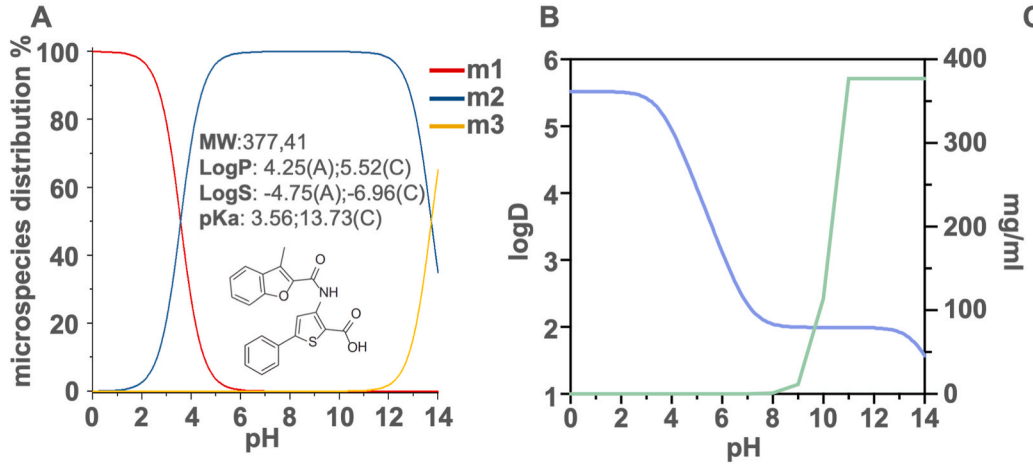

Sample	Yield %
VS10-F	80 ± 20
VS10-AF	50 ± 20
VS10-C	70 ± 20
VS10-AC	60 ± 20
Sample	**HSA (mg/ml)**
VS10-AF	0.37 ± 0.05
VS10-CF	0.25± 0.04

Fig. 1. **A**) VS10 microspecies distribution vs pH; Microspecie n°1 is the neutral one; microspecie n°2 is generated by the dissociation of the carboxylic acid and the n°3 has both the groups dissociated. Inside the figure: VS10 molecular structure and table of inhibitor properties predicted with Chemicalize (C) and ALOGPS 2.1 (A) software (MW molecular weight). **B**) VS10 solubility (green) and logD (blue) trend vs pH. **C**) Table of Nanocrystal dispersion yields (%) and HSA content after the stabilizers exchange protocol (averages and standard deviations are reported).

lipase inhibitor [50], CTAB turned out have a toxicity not negligible even if compared with VS10, therefore in this work we particularly focused on F127 nanocrystals that were used for in vitro and in vivo tests (CTAB data are showed in the supporting information).

Nanocrystals produced with the support of F127 showed a rod shape (Fig. 2A and B). This shape was present also in the drug powder together with filamentous one (Fig. 2C). Therefore, beside the largest dimension i.e. their length, also diameters were measured, and ratios (length/diameter) calculated. The nanocrystallization protocol with the use of F127 promotes the rod shape (filaments are not any more visible in VS10-F and VS10-AF) and decrease the sizes. Indeed, both length and diameters are reducing applying the nanocrystallization protocol including the stabilizers exchange (Fig. S1). The size decrement from VS10-F and VS10-AF is probably due to sonication steps required after centrifugation and lyophilization. Indeed, in Fig. 2B some particles appear as fragments with irregular borders. When CTAB was used, nanocrystals showed an irregular shape with bigger size (largest dimensions 840 ± 40 nm) than crystals obtained by using F127 ($p < 0.0001$) (Fig. S2).

Due to the anisotropy of the particles, DLS hydrodynamic radius is not reliable, it was measured the PdI and Z potential in DPBS. F127 nanocrystals showed negative surface charge (Z: -1.72 mV; PDI: 0.3 ± 0.1) indeed VS10 at neutral pH is monoanionic, then the presence of HSA increases the value (Z: -4.06 mV; 0.3 ± 0.2) because this coating is also negative in the tested condition [51]. VS10-C instead, being covered by a cationic polymer showed a zeta potential of +13.4 mV that after the stabilizers exchange became negative (−10.4 mV) for the HSA presence.

The crystallinity of the nanoparticles was confirmed by XRD spectra containing sharp peaks (Fig. 3A and Fig. S3A). Coating patterns (CTAB, F127, HSA) are not clearly visible through XRD in the respective nanocrystal samples. For both nanocrystals obtained using F127 and CTAB, the formulation protocol changed VS10 crystals' phase. Furthermore, the different morphologies of CTAB and F127 nanocrystals are justified by a different crystalline phase.

The FT-IR spectra of samples (Fig. 3B and Fig. S3B) showed differences among nanocrystal samples and drug powder (VS10-free) while no clear variations arise between surfactant nanocrystals and their respective with HSA. This suggest that spectra changes are not due to stabilizers peak appearance but to crystal differences. Crystalline phases are affecting FT-IR spectra (recorded using powders). Indeed, different intermolecular orientations, affects FT-IR spectra [52,53]. This is visible in Fig. S4 where the spectra of the drug powder and nanocrystals obtained with both surfactants are reported. For VS10-F, the alteration respect to VS10-free are present in the spectral region between 1200 and 1700 cm^{-1}. Also, for VS10-C peaks changes are occurring in this spectral area but this sample showed also a marked intensity increment of peaks between 2800 and 3000 cm^{-1} (without alteration of peak positions). The differences between the sample's spectra between 3000 and 3800 cm^{-1} cannot be considered since the presence of water strongly affects this peak. The spectral range where the majority of the changes are occurring is comprised in the fingerprint region and indeed peaks assignment is intricate, however possible assignations are reported in Table S1 together with spectra differences. For VS10-C, the increased intensity of the two peaks between 2800 and 3000 cm^{-1} might be associated with the presence of CTAB, that being positive could interact through ionic bonds with VS10 forming crystals present as mono anionic microspecies at neutral pH (Fig. 1), and therefore more likely to be present also after the cleaning step. However, no others CTAB peaks are clearly distinguishable in VS10-C and therefore, the crystalline phase role cannot be excluded also in this alteration of the spectra.

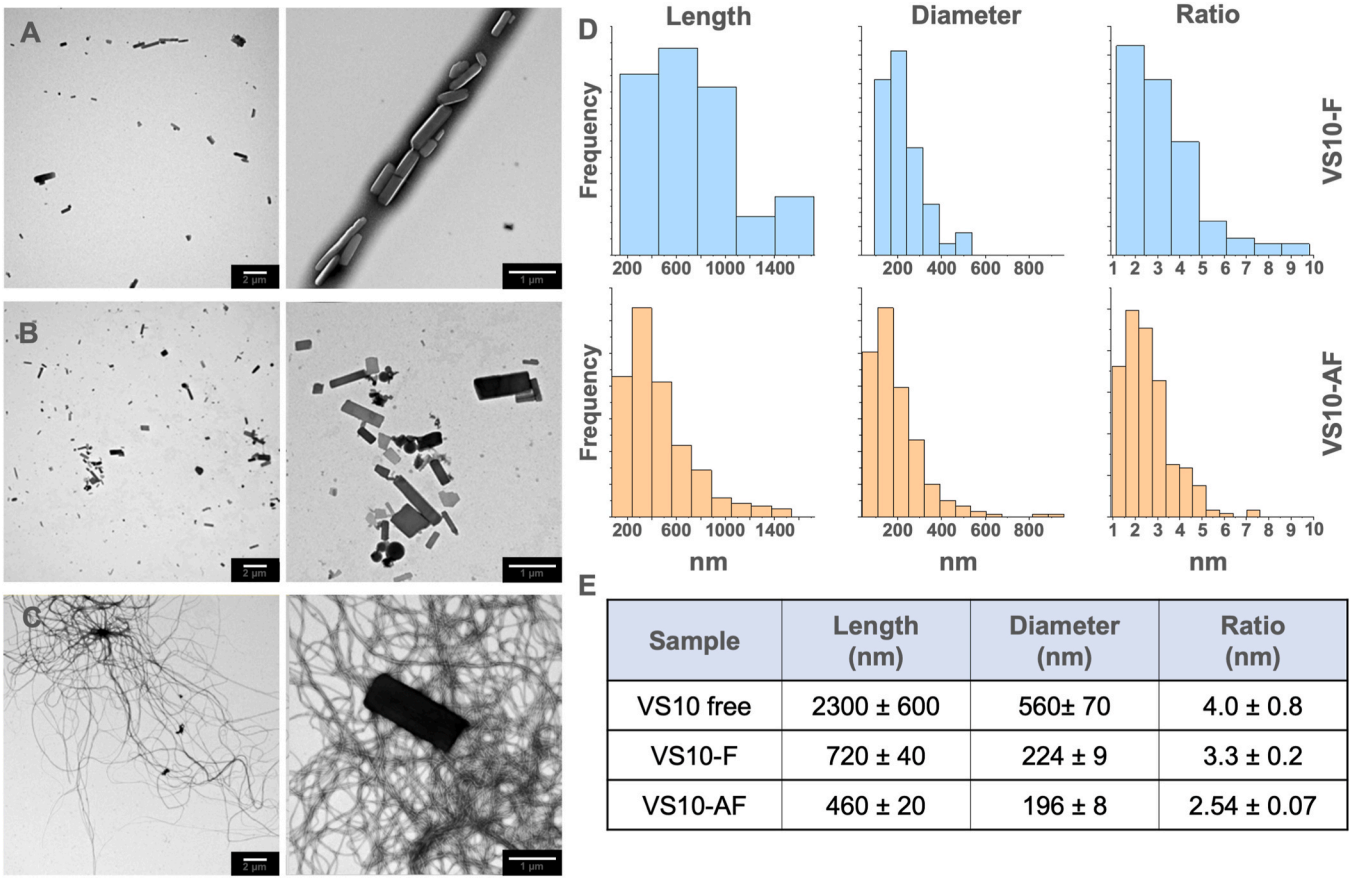

Sample	Length (nm)	Diameter (nm)	Ratio (nm)
VS10 free	2300 ± 600	560± 70	4.0 ± 0.8
VS10-F	720 ± 40	224 ± 9	3.3 ± 0.2
VS10-AF	460 ± 20	196 ± 8	2.54 ± 0.07

Fig. 2. On the left, TEM images and respective size distributions of (**A**) VS10-F, (**B**) VS10-AF and free drug (**C**), obtained by simple dispersion of VS10 powder in MQ water; **D**) Size distributions for VS10-F and VS10-AF determined from TEM pictures. **E**) Table of average dimensions and standard errors of mean are reported.

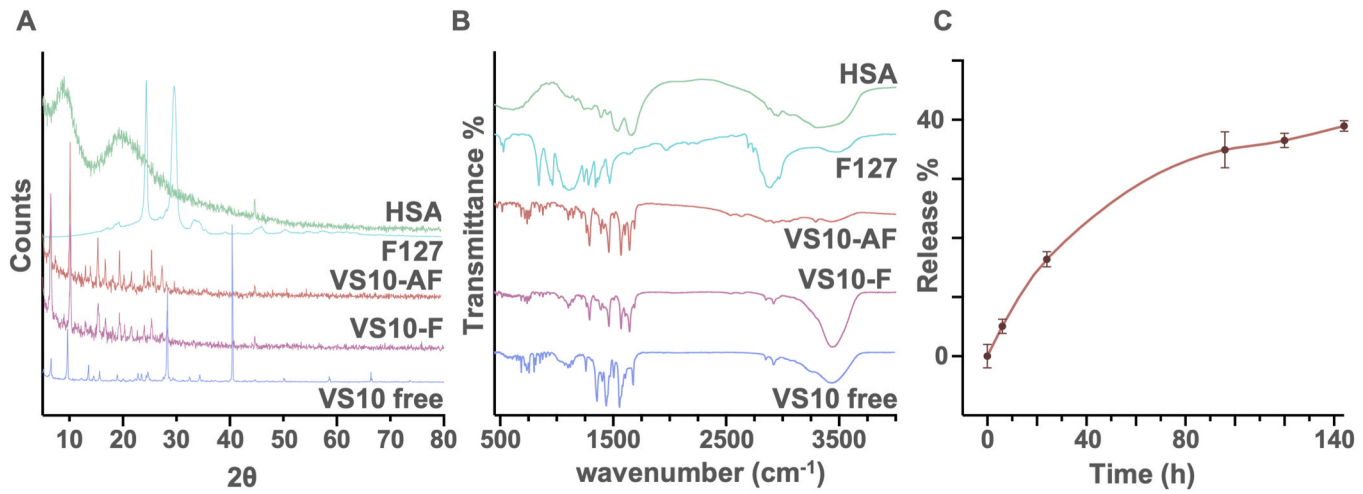

Fig. 3. **A**) XRD and **B**) FT-IR spectra of F127 powder, HSA powder, VS10 free i.e. drug powder, powder of VS10F and VS10-AF. **C**). graph of percentage of released VS10 from VS10-F over time.

In order to further evaluate the chemical stability of VS10 during the formulation protocol, H NMR of drug powder (VS10-free) and VS10-F were compared (Fig. S5). Beside the effect of water content, affecting the peak of the acidic proton of carboxylic acid, the two molecules are comparable. Therefore, the formation of nanocrystals is not altering VS10 molecules and changes visible in FTIR spectra were proved to be caused by sample crystallinity.

3.4. VS10AF exhibits a sustained release profile

In order to evaluate the drug release from nanocrystals, a release test was performed simulating in vivo physiological conditions. As can be seen in Fig. 3C, the release is very slow with 36 ± 1 % of drug released after five days. This tendency to slowly release the drug from the crystalline state is useful to generate a drug depot when administered in vivo, improving the exposure of the cancer cells to the drug.

3.5. VS10AF synergizes with doxorubicin in vitro

In vitro cytotoxic studies were conducted to evaluate the efficacy of VS10, VS10F, and VS10AF. This was achieved by exposing the cancer cell lines (OVCAR5, KURAMOCHI, and SK-OV-3) to progressively

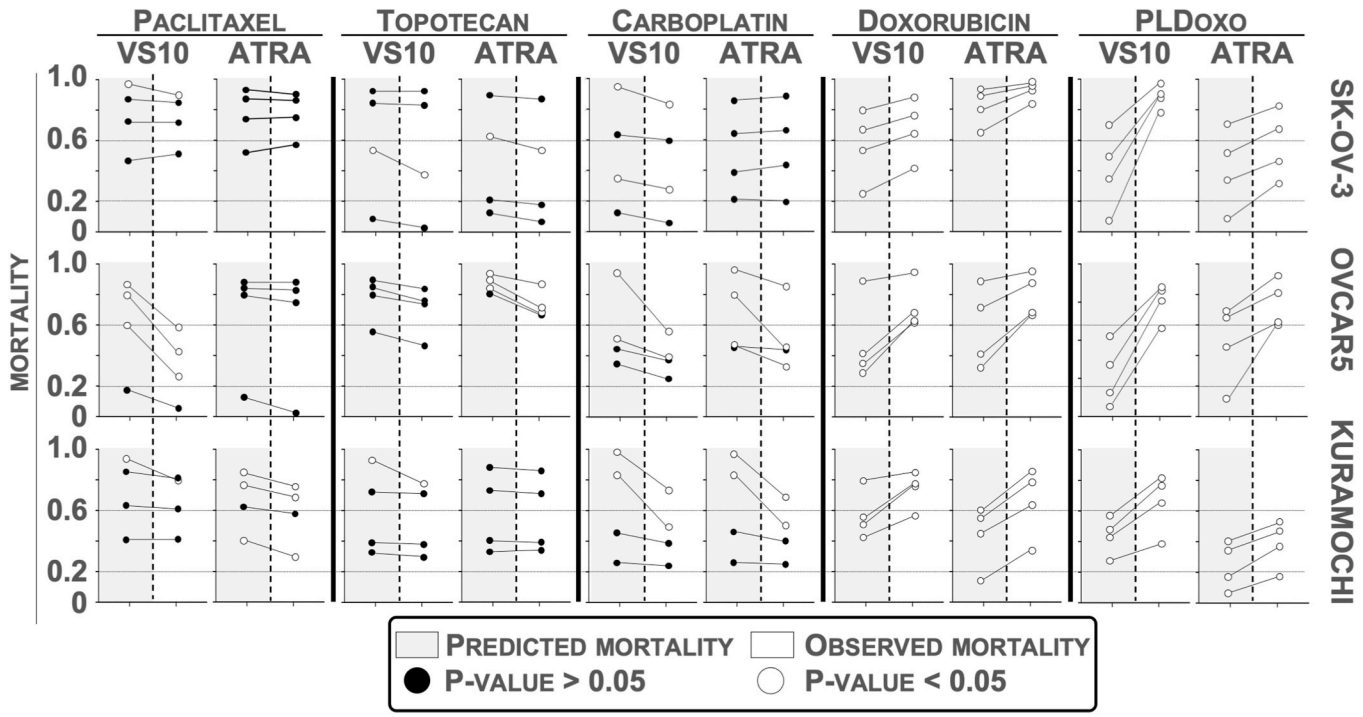

Fig. 4. Synergistic effects of PIN1 inhibitors VS10 and ATRA with standard OC therapies. Data represent the interaction between the PIN1 inhibitors VS10 and ATRA and conventional OC treatments such as paclitaxel, topotecan, carboplatin, doxorubicin, and PLDoxo. The mortality rates, which varies from 0 to 1, are evaluated in two ways: Predicted mortality, calculated using the Bliss independence model for the individual drugs, and Observed mortality, derived from empirical data using a combined drug treatment. Specifically, when observed mortality exceeds predicted mortality, indicate a synergistic effect between the drug pairs. White circles in the graph denote data points with a p-value of <0.05, highlighting statistically significant results. The concentrations used for each combination in this figure are reported in the supplementary material (Supplementary Tables S2–5).

diluted concentrations of these drugs over a 96-h period. The IC50 values for VS10, VS10F, and VS10AF were found to be closely aligned, ranging from 66.1 to 81 μM (Fig. S6). These results suggest that the formulations VS10F and VS10AF maintain the cellular activity of VS10, without altering the cellular uptake or drug-target interaction, while potentially enhancing its delivery.

Second line therapies for HGSOC are ineffective and rely mostly on patient compliance. The potential of PIN1 inhibitors to enhance second-line therapies of HGSOC was investigated through in vitro screenings conducted on OC cell lines, including OVCAR5, KURAMOCHI, and SK-OV-3. The study focused on assessing the synergistic effects of combining PIN1 inhibitors, specifically VS10 and ATRA [34], with conventional therapeutics such as paclitaxel, topotecan, carboplatin, doxorubicin, and PLDoxo. The results indicated a limited synergistic interaction between PIN1 inhibitors and the majority of the tested drugs, with notable exceptions being doxorubicin and PLDoxo, where the observed mortality rates were significantly different from those predicted by the Bliss independence model (Fig. 4).

Additionally, the synergistic interactions between doxorubicin, PLDoxo, and the VS10AF formulation were investigated to ascertain if the drug delivery system influenced the efficacy of free VS10. The studies confirmed a synergistic relationship (Fig. S7).

To further investigate the mechanisms underlying the observed synergism, we assessed apoptosis and DNA damage in the combination treatments by measuring Caspase 3/7 activity and γH2A.X activation.

The results demonstrated that the drug combinations induced a stronger Caspase 3/7 activation at 48 and 72 h (Fig. 5), together with an increased γH2A.X signal at 24 h (Fig. 6), compared to single treatments.

3.6. VS10AF improves second line therapy of HGSOC

A HGSOC model has been obtained by injecting OVCAR5 cell lines subcutaneously into the flanks of nude mice. Mice were treated with VS10AF (12.5 mg/kg), PLDoxo (1.5 mg/kg), and the drug combination VS10AF-PLDoxo when the tumors reached the size of about 34 ± 12 mm^3. The drug combination VS10-PLDoxo treatment resulted in a significant reduction of the tumor volume compared to control and single treatments (Fig. 7A). Hence, the body weight of the mice did not show any significant changes between the different treatment conditions (Fig. 7B). Histopathological analysis showed that even at cellular levels, there are no signs of toxicity (Fig. 7C).

4. Conclusions

In this study, we report the successful development and comprehensive characterization of VS10 nanocrystals as a novel formulation strategy for the selective delivery of a PIN1 inhibitor in HGSOC. Nanocrystal technology offers a carrier-free drug delivery platform, reducing the risk of excipient-induced toxicity, and is particularly advantageous for poorly soluble small molecules such as VS10. The nanocrystallization process preserved the chemical identity of the drug, as proved by the characterization and as confirmed by in vitro cytotoxicity studies across multiple ovarian cancer cell lines with IC_{50} values for VS10, VS10F, and VS10AF closely aligned, indicating that neither the formulation process nor surface stabilization interfered with cellular uptake or drug-target interaction. Nanocrystals stabilization with human serum albumin, achieved through surfactant exchange, aimed to enhance the colloidal stability and biocompatibility and possibly improve tumor selectivity of the particles.

OC treatment has long relied on chemotherapy, especially platinum-based drugs like carboplatin, which are initially effective for many patients. However, recurrence is common, and tumors often develop resistance, known as platinum resistance, making subsequent treatments less effective and more focused on slowing the progress of the disease than ending it. Second-line therapy for OC, particularly in cases of platinum-resistant HGSOC, faces several limitations. While initial treatments with platinum-based chemotherapy can be effective, most patients eventually experience recurrence, and tumors often develop resistance, making subsequent treatments less effective. Current second-line options, such as PLDoxo, topotecan, and paclitaxel, show only modest efficacy, typically providing short-term disease control but rarely long-term remission. Additionally, tumor heterogeneity also contributes to treatment resistance, while the limited success of immunotherapy in OC highlights the difficulty of overcoming the tumor's immunosuppressive environment. As a result, second-line therapies often focus on palliative care rather than curative intent, leading to a need for novel treatment strategies to address these challenges and improve patient outcomes.

In response to these limitations, a new wave of therapies is emerging. PARP inhibitors have brought significant progress, particularly for patients with BRCA mutations or homologous recombination deficiencies, by blocking cancer cells' ability to repair DNA [54]. Yet, their benefits are limited to specific genetic profiles. New hope is also coming from antibody-drug conjugates (ADCs) like mirvetuximab soravtansine [55], which target overexpressed proteins on cancer cells and deliver

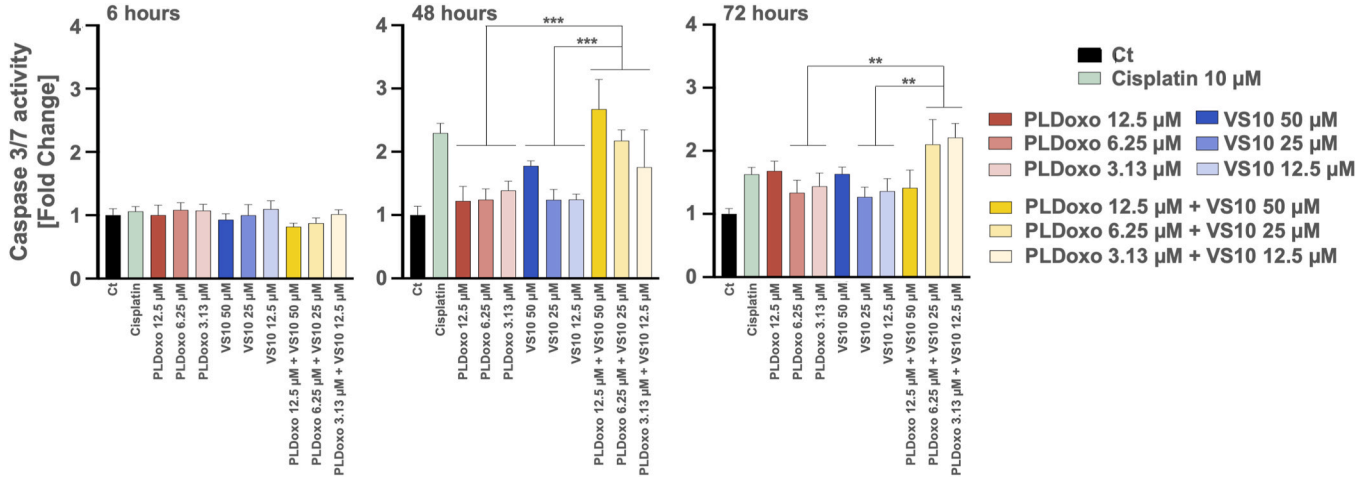

Fig. 5. Synergistic treatment between VS10 and PLDoxo induces caspase 3/7 activation. SK-OV-3 cells were treated with PLDoxo, VS10, and their combinations. Untreated cells were used as negative control, while cisplatin was included as positive control. Caspase activity was assessed at 6, 48 and 72 h post-treatment and data were normalized to the luminescence of untreated controls. Statistical analyses were performed among single and double drug combinations at the same concentration. A significant increase in caspase activation was observed in the combination groups compared to single treatments.

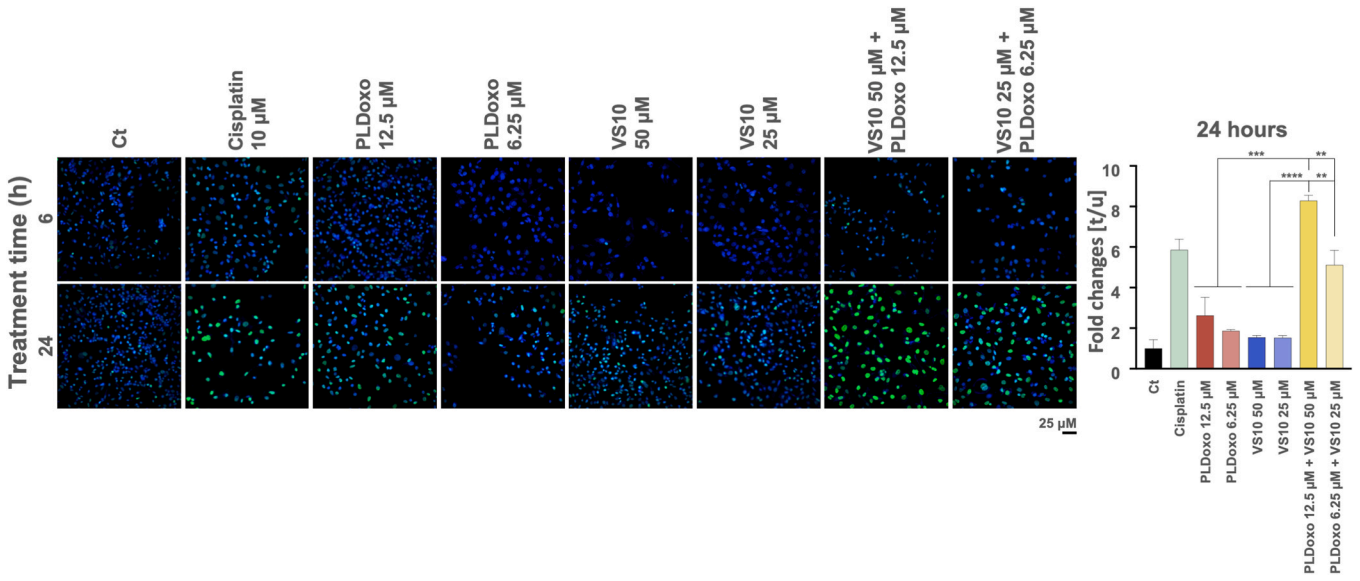

Fig. 6. Synergistic treatment between VS10 and PLDoxo enhance γH2A.X activation. SK-OV-3 cells were treated with PLDoxo, VS10 and their combinations. Untreated cells were used as negative control, and cisplatin was included as positive control. Images were acquired using a Nikon Eclipse Ti2 equipped with an X-Light V2 L-FOV spinning disk confocal system. Phospho-Histone H2A.X (Ser139) green signals increase in the double drug combination compared to single treatments. Nuclei are in blue. Signal intensity quantification was performed on three independent biological replicates. Statistical significance was calculated between single treatments and the combination at the respective concentrations. Data (t) were normalized to untreated controls (u).

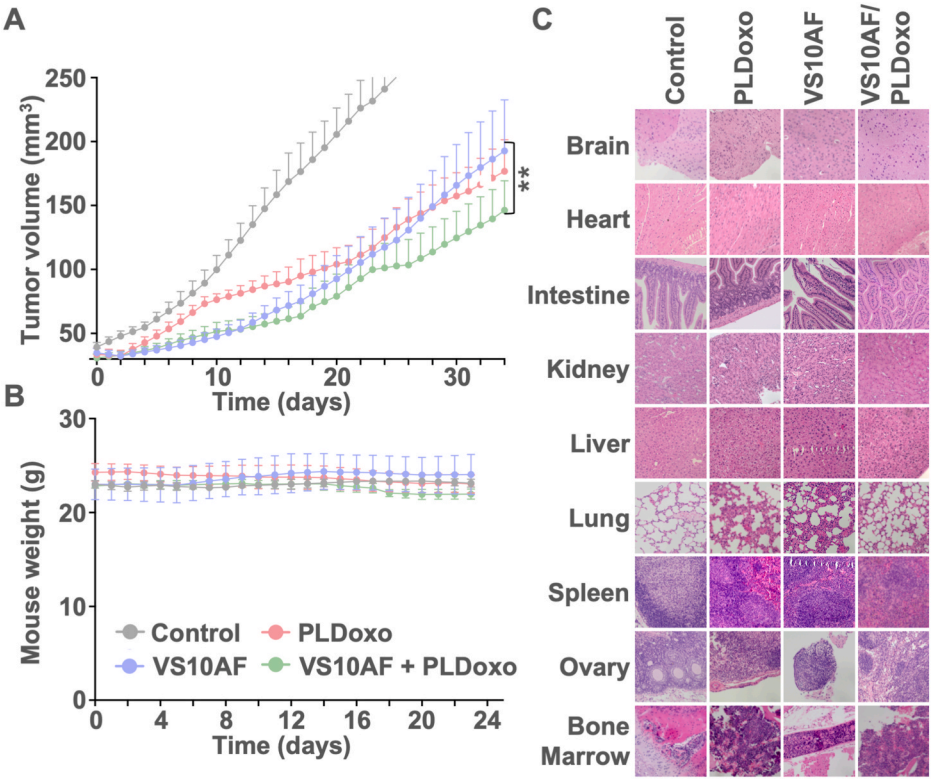

Fig. 7. Enhanced effectiveness of PLDoxo when combined with VS10AF in a HGSOC mouse tumor model. This figure illustrates the results from an experiment where 5 x 10^6 cells OVCAR5 cell line was injected into nude mice, with each treatment group consisting of eight tumors. **A**) Illustrates the measurement of tumor volume over a period of 34 days under different treatment regimes. **B**) Monitoring of body weight, providing an indication of the systemic impact of the treatments. **C**) Hematoxylin and Eosin (H&E) staining of tissue sections post-treatment, which was conducted to assess the morphological changes in the tissues after administration of PLDoxo, VS10AF, and a combination of VS10AF and PLDoxo. This comprehensive data set underscores the potential of VS10AF to enhance the effectiveness of PLDoxo, while also indicating its systemic tolerability in a relevant in vivo condition.

chemotherapy directly to them offering a promising option for platinum-resistant cases. Given the limited efficacy and patient compliance challenges associated with current second-line options, targeting PIN1, a prolyl isomerase involved in multiple oncogenic signaling pathways, could enhance therapeutic response.

The molecular characteristics of PIN1 offer several key features that make it an attractive target for improving the limitations of second-line OC therapies. PIN1 is an enzyme that catalyzes the isomerization of phosphorylated serine/threonine-proline bonds in proteins, a process that can alter the conformation and function of numerous key signaling molecules involved in cell cycle regulation, DNA damage repair, and oncogenic pathways. PIN1 is a critical regulator of several pathways that control cell survival, proliferation, and DNA repair. It influences key proteins involved in the cell cycle, such as p53, Cyclin D1, and NF-kB, and plays a role in the activation of oncogenic pathways (e.g., AKT, MAPK, Wnt/β-catenin). By modulating these pathways, PIN1 supports the growth and survival of cancer cells, including those resistant to chemotherapy [56].

PIN1 interacts with key players in the DNA damage response, such as BRCA1, ATM, and CHK1, which are crucial for maintaining genomic stability. By modulating these proteins, PIN1 influences the ability of cancer cells to repair DNA damage induced by chemotherapy. Inhibiting PIN1 can potentially impair DNA repair mechanisms, making tumor cells more susceptible to chemotherapy-induced DNA damage [57]. In line with this rationale, our experiments showed that the combination of VS10 with PLDoxo induced an earlier and stronger activation of γH2AX, a marker of DNA double-strand breaks, as well as Caspase 3/7 activity, compared to either treatment alone. These results confirm that the enhanced efficacy of the combination is mechanistically associated with increased DNA damage accumulation and apoptosis, supporting the hypothesis that PIN1 inhibition may sensitizes ovarian cancer cells to doxorubicin by impairing DNA repair and survival signaling.

Recent studies have demonstrated the therapeutic potential of PIN1 inhibition as a chemosensitizing strategy across a range of malignancies. In pancreatic cancer models, PIN1 inhibition combined with gemcitabine and anti-PD-1 immune checkpoint blockade resulted in significantly enhanced tumor regression and immune activation compared to monotherapies, highlighting the capacity of PIN1 targeting to potentiate both cytotoxic and immunotherapeutic responses [58]. In castration-resistant prostate cancer xenograft models, co-treatment with the PIN1 inhibitor juglone and the androgen receptor antagonist ralaniten produced synergistic antitumor effects by inducing cell cycle arrest and disrupting PIN1-dependent transcriptional activity [59]. In hepatocellular carcinoma, PIN1 inhibition was shown to augment the efficacy of sorafenib, promoting apoptosis and reducing tumor burden in vivo [60]. Similarly, in colorectal cancer, PIN1 targeting enhanced cellular sensitivity to 5-fluorouracil (5-FU), supporting the rationale for combination regimens aimed at overcoming chemotherapy resistance [61]. In gastric cancer, PIN1 inhibition sensitized tumor cells to standard chemotherapeutic agents, with overexpression of PIN1 correlating with poor clinical outcomes, thus reinforcing its role as a negative prognostic marker and therapeutic target [62]. Although ATRA exerts multi-targeted effects, its combination with mitochondrial-targeted lonidamine or doxorubicin may offer a promising strategy for enhancing therapeutic efficacy in breast cancer treatment [63,64].

In vitro combination studies have shown that VS10 exhibit modest synergy with most standard chemotherapy agents, but strong synergistic effects are observed in combination with doxorubicin and PLDoxo, suggesting a potential role for PIN1 inhibition in improving the efficacy of these agents. Importantly, the synergistic interaction between VS10AF and PLDoxo was maintained in vivo using an xenograft ovarian cancer model. Mice treated with the VS10AF–PLDoxo combination exhibited a significant reduction in tumor volume relative to single-agent treatments, without observable systemic toxicity or weight loss. Histopathological evaluation confirmed the absence of tissue damage, supporting the safety profile of this combination. These findings not only validate PIN1 as a relevant target in OC but also underscore the value of nanocrystal formulations in enhancing therapeutic efficacy. From a clinical perspective, PLDoxo is utilized as a standard second-line agent for recurrent ovarian cancer, particularly in platinum-resistant cases. However, its efficacy is limited, and resistance frequently develops, especially after PARP inhibitor therapy. In this context, PIN1 inhibition represents a promising strategy to overcome resistance mechanisms by impairing DNA repair and promoting apoptosis. The favorable safety profile of VS10AF combined with PLDoxo observed in vivo supports its potential integration into existing treatment paradigms, either as a strategy to improve responses in platinum-resistant HGSOC or as a complementary option following PARP inhibitor failure.

Taken together, this work demonstrates the feasibility of using a nanocrystal-based approach to deliver VS10 and provides the first evidence of synergistic antitumor activity when combined with PLDoxo. The data supports further preclinical development of VS10AF as a combination partner in second-line ovarian cancer therapy and pave the way for future clinical studies aimed at evaluating this combination in patients with limited treatment options.

CRediT authorship contribution statement

Gloria Saorin: Writing – review & editing, Writing – original draft, Visualization, Software, Methodology, Investigation, Formal analysis, Data curation, Conceptualization. **Matteo Mauceri:** Writing – review & editing, Writing – original draft, Visualization, Validation, Software, Methodology, Investigation, Formal analysis, Data curation, Conceptualization. **Isabella Caligiuri:** Writing – review & editing, Supervision, Conceptualization. **Urska Kamensek:** Writing – review & editing, Investigation, Data curation. **Simona Kranjc Brezar:** Writing – review & editing, Investigation, Data curation. **Giuseppe Corona:** Investigation, Data curation. **Ombretta Repetto:** Investigation, Data curation. **Tiziana Perin:** Investigation, Formal analysis. **Gabriele Grassi:** Writing – review & editing. **Carlotta Granchi:** Writing – review & editing, Investigation. **Tiziano Tuccinardi:** Writing – review & editing, Investigation. **Maja Cemazar:** Writing – review & editing, Data curation. **Vincenzo Canzonieri:** Writing – review & editing, Supervision, Resources, Investigation. **Muhammad Adeel:** Investigation, Conceptualization. **Flavio Rizzolio:** Writing – review & editing, Supervision, Resources, Funding acquisition, Conceptualization.

Disclaimer

This manuscript has undergone grammar and syntax correction using ChatGPT, an AI language model developed by OpenAI. While every effort has been made to improve the clarity and accuracy of the language in this document, the authors acknowledge that the final content and scientific interpretations remain the sole responsibility of the authors and their collaborators. ChatGPT has been used exclusively to enhance the manuscript's readability and expression, and not to generate any type of data.

Funding acquisition

This research was funded to F.R. by Associazione Italiana per la Ricerca sul Cancro (AIRC, IG 23566) and V.C., G.C., O.R., Ricerca Corrente and I.C. 5‰ Ricerca Sanitaria by Ministry of health (Italy), M.C.. This research was partially funded by the Slovenian Research and Innovation Agency (Program No P3-0003)

Declaration of competing interest

The authors declare that they have no known competing financial interests or personal relationships that could have appeared to influence the work reported in this paper.

Appendix A. Supplementary data

Supplementary data to this article can be found online at https://doi.org/10.1016/j.canlet.2025.218128.

Data availability

The data supporting the findings of this study are available in the paper, supplementary information files, and can be obtained from the corresponding authors upon reasonable request.

References

[1] C. Mattiuzzi, G. Lippi, Current cancer epidemiology, J. Epidemiol. Glob. Health 9 (2019) 217–222, https://doi.org/10.2991/jegh.k.191008.001.

[2] V.L. Seltzer, Ovarian cancer, in: Cancer Screening, CRC Press, 2021, pp. 431–440, https://doi.org/10.1201/9780429179587-19.

[3] A. Saorin, E. Di Gregorio, G. Miolo, A. Steffan, G. Corona, Emerging role of metabolomics in ovarian cancer diagnosis, Metabolites 10 (2020) 1–15, https://doi.org/10.3390/metabo10100419.

[4] S. Boussios, G. Zarkavelis, E. Seraj, I. Zerdes, K. Tatsi, G. Pentheroudakis, Non-epithelial ovarian cancer: elucidating uncommon gynaecological malignancies, Anticancer Res. 36 (2016) 5031–5042, https://doi.org/10.21873/anticanres.11072.

[5] M.-A. Lisio, L. Fu, A. Goyeneche, Z. Gao, C. Telleria, High-grade serous ovarian cancer: basic sciences, clinical and therapeutic standpoints, Int. J. Mol. Sci. 20 (2019) 952, https://doi.org/10.3390/ijms20040952.

[6] E. Pujade-Lauraine, S. Banerjee, S. Pignata, Management of platinum-resistant, relapsed epithelial ovarian cancer and new drug perspectives, J. Clin. Oncol. 37 (2019) 2437–2448, https://doi.org/10.1200/JCO.19.00194.

[7] J. Naghinezhad, S. Moradpanah, N. Khodakarim, M.R. Hamblin, H. Rezaeeyan, Nanodrug-based modulation of platelet–leukocyte interactions in ovarian cancer: a new frontier in targeted therapy, Cancer Nanotechnol. 16 (2025) 1–23, https://doi.org/10.1186/S12645-025-00340-3/FIGURES/2.

[8] A. Saorin, G. Saorin, F. Duzagac, P. Parisse, N. Cao, G. Corona, E. Cavarzerani, F. Rizzolio, Microfluidic production of amiodarone loaded nanoparticles and application in drug repositioning in ovarian cancer, Sci. Rep. 14 (2024) 1–18, https://doi.org/10.1038/S41598-024-55801-3. SUBJMETA.

[9] L. Wang, Q. Zhang, X. Wang, Z. Dong, S. Liu, Q. Wang, Z. Zhang, J. Xing, Therapeutic landscape of ovarian cancer: recent advances and emerging therapies, Biomark. Res. 13 (2025), https://doi.org/10.1186/S40364-025-00818-7.

[10] A. Zannini, A. Rustighi, E. Campaner, G. Del Sal, Oncogenic hijacking of the PIN1 signaling network, Front. Oncol. 9 (2019), https://doi.org/10.3389/fonc.2019.00094.

[11] C.W. Cheng, E. Tse, PIN1 in cell cycle control and cancer, Front. Pharmacol. 9 (2018), https://doi.org/10.3389/fphar.2018.01367.

[12] Y.-C. Liou, A. Ryo, H.-K. Huang, P.-J. Lu, R. Bronson, F. Fujimori, T. Uchida, T. Hunter, K.P. Lu, Loss of Pin1 function in the mouse causes phenotypes resembling cyclin D1-null phenotypes, Proc. Natl. Acad. Sci. U. S. A. 99 (2002) 1335–1340, https://doi.org/10.1073/pnas.032404099.

[13] F. Rizzolio, C. Lucchetti, I. Caligiuri, I. Marchesi, M. Caputo, A.J. Klein-Szanto, L. Bagella, M. Castronovo, A. Giordano, Retinoblastoma tumor-suppressor protein phosphorylation and inactivation depend on direct interaction with Pin1, Cell Death Differ. 19 (2012) 1152–1161, https://doi.org/10.1038/cdd.2011.202.

[14] F. Rizzolio, I. Caligiuri, C. Lucchetti, R. Fratamico, V. Tomei, G. Gallo, A. Agelan, G. Ferrari, G. Toffoli, A.J. Klein-Szanto, A. Giordano, Dissecting Pin1 and phospho-pRb regulation, J. Cell. Physiol. 228 (2013) 73–77, https://doi.org/10.1002/jcp.24107.

[15] A. Ryo, M. Nakamura, G. Wulf, Y.-C. Liou, K.P. Lu, Pin1 regulates turnover and subcellular localization of β-catenin by inhibiting its interaction with APC, Nat. Cell Biol. 3 (2001) 793–801, https://doi.org/10.1038/ncb0901-793.

[16] P. Zacchi, M. Gostissa, T. Uchida, C. Salvagno, F. Avolio, S. Volinia, Z. Ronai, G. Blandino, C. Schneider, G. Del Sal, The prolyl isomerase Pin1 reveals a mechanism to control p53 functions after genotoxic insults, Nature 419 (2002) 853–857, https://doi.org/10.1038/nature01120.

[17] A.S. Farrell, C. Pelz, X. Wang, C.J. Daniel, Z. Wang, Y. Su, M. Janghorban, X. Zhang, C. Morgan, S. Impey, R.C. Sears, Pin1 regulates the dynamics of c-Myc DNA binding to facilitate target gene regulation and oncogenesis, Mol. Cell Biol. 33 (2013) 2930–2949, https://doi.org/10.1128/MCB.01455-12.

[18] J. Long, J. Wang, Y. Dong, J. Yang, G. Xie, Y. Tong, Prolyl isomerase Pin1 promotes autophagy and cancer cell viability through activating FoxO3 signalling, Cell. Signal. 113 (2024), https://doi.org/10.1016/j.cellsig.2023.110940.

[19] A. Rustighi, A. Zannini, E. Campaner, Y. Ciani, S. Piazza, G. Del Sal, PIN1 in breast development and cancer: a clinical perspective, Cell Death Differ. 24 (2017) 200–211, https://doi.org/10.1038/cdd.2016.122.

[20] G. Ayala, D. Wang, G. Wulf, A. Frolov, R. Li, J. Sowadski, T.M. Wheeler, K.P. Lu, L. Bao, The prolyl isomerase Pin1 is a novel prognostic marker in human prostate cancer, Cancer Res. 63 (2003) 6244–6251.

[21] C. Lucchetti, I. Caligiuri, G. Toffoli, A. Giordano, F. Rizzolio, The prolyl isomerase Pin1 acts synergistically with CDK2 to regulate the basal activity of estrogen receptor α in breast cancer, PLoS One 8 (2013) e55355, https://doi.org/10.1371/journal.pone.0055355.

[22] R. La Montagna, I. Caligiuri, P. Maranta, C. Lucchetti, L. Esposito, M.G. Paggi, G. Toffoli, F. Rizzolio, A. Giordano, Androgen receptor serine 81 mediates Pin1 interaction and activity, Cell Cycle 11 (2012) 3415–3420, https://doi.org/10.4161/cc.21730.

[23] C. Russo Spena, L. De Stefano, S. Palazzolo, B. Salis, C. Granchi, F. Minutolo, T. Tuccinardi, R. Fratamico, S. Crotti, S. D'Aronco, M. Agostini, G. Corona, I. Caligiuri, V. Canzonieri, F. Rizzolio, Liposomal delivery of a Pin1 inhibitor complexed with cyclodextrins as new therapy for high-grade serous ovarian cancer, J. Contr. Release 281 (2018) 1–10, https://doi.org/10.1016/j.jconrel.2018.04.055.

[24] G. Wulf, P. Garg, Y.-C. Liou, D. Iglehart, K.P. Lu, Modeling breast cancer in vivo and ex vivo reveals an essential role of Pin1 in tumorigenesis, EMBO J. 23 (2004) 3397–3407, https://doi.org/10.1038/sj.emboj.7600323.

[25] F. Suizu, A. Ryo, G. Wulf, J. Lim, K.P. Lu, Pin1 regulates centrosome duplication, and its overexpression induces centrosome amplification, chromosome instability, and oncogenesis, Mol. Cell Biol. 26 (2006) 1463–1479, https://doi.org/10.1128/MCB.26.4.1463-1479.2006.

[26] K.P. Lu, F. Suizu, X.Z. Zhou, G. Finn, P. Lam, G. Wulf, Targeting carcinogenesis: a role for the prolyl isomerase Pin1? Mol. Carcinog. 45 (2006) 397–402, https://doi.org/10.1002/mc.20216.

[27] Y.M. Lee, Y.C. Liou, Gears-in-motion: the interplay of WW and PPIase domains in PIN1, Front. Oncol. 8 (2018), https://doi.org/10.3389/fonc.2018.00469.

[28] R. Kanaoka, A. Kushiyama, Y. Seno, Y. Nakatsu, Y. Matsunaga, T. Fukushima, Y. Tsuchiya, H. Sakoda, M. Fujishiro, T. Yamamotoya, H. Kamata, A. Matsubara, T. Asano, Pin1 inhibitor juglone exerts anti-oncogenic effects on LNCaP and DU145 cells despite the patterns of gene regulation by Pin1 differing between these cell lines, PLoS One 10 (2015), https://doi.org/10.1371/journal.pone.0127467 e0127467–e0127467.

[29] J. Wang, K. Liu, X.F. Wang, D.J. Sun, Juglone reduces growth and migration of U251 glioblastoma cells and disrupts angiogenesis, Oncol. Rep. 38 (2017) 1959–1966, https://doi.org/10.3892/or.2017.5878.

[30] N.Y. Lee, H.-K. Choi, J.-H. Shim, K.-W. Kang, Z. Dong, H.S. Choi, The prolyl isomerase Pin1 interacts with a ribosomal protein S6 kinase to enhance insulin-induced AP-1 activity and cellular transformation, Carcinogenesis 30 (2009) 671–681, https://doi.org/10.1093/carcin/bgp027.

[31] C. Wang, Y. Zhao, Y. Peng, W. Chen, J. Zhu, C. Gu, R. Huo, L. Ding, Y. Liu, T. Liu, C. Zhang, W. Yang, H. Wang, W. Guo, B. Wang, Juglone induces ferroptotic effect on hepatocellular carcinoma and pan-cancer via the FOSL1-HMOX1 axis, Phytomedicine 139 (2025), https://doi.org/10.1016/j.phymed.2025.156417.

[32] D. Erkoc-Kaya, H. Arikoglu, E. Guclu, D. Dursunoglu, E. Menevse, Juglone-ascorbate treatment enhances reactive oxygen species mediated mitochondrial apoptosis in pancreatic cancer, Mol. Biol. Rep. 51 (2024), https://doi.org/10.1007/S11033-024-09254-6.

[33] J. Zhong, Y. Hua, S. Zou, B. Wang, Juglone triggers apoptosis of non-small cell lung cancer through the reactive oxygen species -mediated PI3K/Akt pathway, PLoS One 19 (2024), https://doi.org/10.1371/JOURNAL.PONE.0299921.

[34] S. Wei, S. Kozono, L. Kats, M. Nechama, W. Li, J. Guarnerio, M. Luo, M.-H. You, Y. Yao, A. Kondo, H. Hu, G. Bozkurt, N.J. Moerke, S. Cao, M. Reschke, C.-H. Chen, E.M. Rego, F. Lo-Coco, L.C. Cantley, T.H. Lee, H. Wu, Y. Zhang, P.P. Pandolfi, X. Z. Zhou, K.P. Lu, Active Pin1 is a key target of all-trans retinoic acid in acute promyelocytic leukemia and breast cancer, Nat. Med. 21 (2015) 457–466, https://doi.org/10.1038/nm.3839.

[35] X.-H. Liao, A.L. Zhang, M. Zheng, M.-Q. Li, C.P. Chen, H. Xu, Q.-S. Chu, D. Yang, W. Lu, T.-F. Tsai, H. Liu, X.Z. Zhou, K.P. Lu, Chemical or genetic Pin1 inhibition exerts potent anticancer activity against hepatocellular carcinoma by blocking multiple cancer-driving pathways, Sci. Rep. 7 (2017) 43639, https://doi.org/10.1038/srep43639.

[36] K. Wang, X. Qiu, Z. Zhang, H. Xu, Y. Tan, R. Su, F. Gao, J. Zhuo, W. Li, Z. Lian, H. He, X. Xu, ATRA sensitized the response of hepatocellular carcinoma to sorafenib by downregulation of p21-activated kinase 1, Cell Commun. Signal. 21 (2023) 193, https://doi.org/10.1186/s12964-023-01194-1.

[37] S. Kozono, Y.-M. Lin, H.-S. Seo, B. Pinch, X. Lian, C. Qiu, M.K. Herbert, C.-H. Chen, L. Tan, Z.J. Gao, W. Massefski, Z.M. Doctor, B.P. Jackson, Y. Chen, S. Dhe-Paganon, K.P. Lu, X.Z. Zhou, Arsenic targets Pin1 and cooperates with retinoic acid to inhibit cancer-driving pathways and tumor-initiating cells, Nat. Commun. 9 (2018) 3069, https://doi.org/10.1038/s41467-018-05402-2.

[38] J. Leung, A. Pang, W.-H. Yuen, Y.-L. Kwong, E.W.C. Tse, Relationship of expression of aquaglyceroporin 9 with arsenic uptake and sensitivity in leukemia cells, Blood 109 (2007) 740–746, https://doi.org/10.1182/blood-2006-04-019588.

[39] E. Campaner, A. Rustighi, A. Zannini, A. Cristiani, S. Piazza, Y. Ciani, O. Kalid, G. Golan, E. Baloglu, S. Shacham, B. Valsasina, U. Cucchi, A.C. Pippione, M.L. Lolli, B. Giabbai, P. Storici, P. Carloni, G. Rossetti, F. Benvenuti, E. Bello, M. D'Incalci, E. Cappuzzello, A. Rosato, G. Del Sal, A covalent PIN1 inhibitor selectively targets cancer cells by a dual mechanism of action, Nat. Commun. 8 (2017) 15772, https://doi.org/10.1038/ncomms15772.

[40] C. Russo Spena, L. De Stefano, G. Poli, C. Granchi, M. El Boustani, F. Ecca, G. Grassi, M. Grassi, V. Canzonieri, A. Giordano, T. Tuccinardi, I. Caligiuri, F. Rizzolio, Virtual screening identifies a PIN1 inhibitor with possible antiovarian cancer effects, J. Cell. Physiol. 234 (2019) 15708–15716, https://doi.org/10.1002/jcp.28224.

[41] C. Guo, X. Hou, L. Dong, J. Marakovits, S. Greasley, E. Dagostino, R. Ferre, M. C. Johnson, P.S. Humphries, H. Li, G.D. Paderes, J. Piraino, E. Kraynov, B. W. Murray, Structure-based design of novel human Pin1 inhibitors (III): optimizing affinity beyond the phosphate recognition pocket, Bioorg. Med. Chem. Lett. 24 (2014) 4187–4191, https://doi.org/10.1016/j.bmcl.2014.07.044.

[42] G. Saorin, M. Mauceri, E. Cavarzerani, I. Caligiuri, G. Bononi, C. Granchi, M. Bartoletti, T. Perin, T. Tuccinardi, V. Canzonieri, A. Muhammad, F. Rizzolio,

Enhanced activity of a pluronic F127 formulated Pin1 inhibitor for ovarian cancer therapy, J. Drug Deliv. Sci. Technol. (2023) 104718, https://doi.org/10.1016/j.jddst.2023.104718.
[43] B. Rossier, O. Jordan, E. Allémann, C. Rodríguez-Nogales, Nanocrystals and nanosuspensions: an exploration from classic formulations to advanced drug delivery systems, Drug Deliv. Transl. Res. 14 (2024) 3438–3451, https://doi.org/10.1007/S13346-024-01559-0/FIGURES/4.
[44] E.N. Hoogenboezem, C.L. Duvall, Harnessing albumin as a carrier for cancer therapies, Adv. Drug Deliv. Rev. 130 (2018) 73–89, https://doi.org/10.1016/j.addr.2018.07.011.
[45] C. Li, X. Wang, H. Song, S. Deng, W. Li, J. Li, J. Sun, Current multifunctional albumin-based nanoplatforms for cancer multi-mode therapy, Asian J. Pharm. Sci. 15 (2020) 1–12, https://doi.org/10.1016/j.ajps.2018.12.006.
[46] A. Parodi, J. Miao, S. Soond, M. Rudzińska, A. Zamyatnin, Albumin nanovectors in cancer therapy and imaging, Biomolecules 9 (2019) 218, https://doi.org/10.3390/biom9060218.
[47] G. Stehle, H. Sinn, A. Wunder, H.H. Schrenk, J.C.M. Stewart, G. Hartung, W. Maier-Borst, D.L. Heene, Plasma protein (albumin) catabolism by the tumor itself—implications for tumor metabolism and the genesis of cachexia, Crit. Rev. Oncol. Hematol. 26 (1997) 77–100, https://doi.org/10.1016/S1040-8428(97)00015-2.
[48] J. Park, B. Sun, Y. Yeo, Albumin-coated nanocrystals for carrier-free delivery of paclitaxel, J. Contr. Release 263 (2017) 90–101, https://doi.org/10.1016/j.jconrel.2016.12.040.
[49] C.I. Bliss, The toxicity of poisons applied jointly, Ann. Appl. Biol. 26 (1939) 585–615, https://doi.org/10.1111/j.1744-7348.1939.tb06990.x.
[50] M. Adeel, G. Saorin, G. Boccalon, A.A. Sfriso, S. Parisi, I. Moro, S. Palazzolo, I. Caligiuri, C. Granchi, G. Corona, M. Cemazar, V. Canzonieri, T. Tuccinardi, F. Rizzolio, A carrier free delivery system of a monoacylglycerol lipase hydrophobic inhibitor, Int. J. Pharm. 613 (2022) 121374, https://doi.org/10.1016/j.ijpharm.2021.121374.
[51] K. Baler, O.A. Martin, M.A. Carignano, G.A. Ameer, J.A. Vila, I. Szleifer, Electrostatic unfolding and interactions of albumin driven by pH changes: a molecular dynamics study, J. Phys. Chem. B 118 (2014) 921–930, https://doi.org/10.1021/jp409936v.
[52] Y. He, Y. Inoue, Novel FTIR method for determining the crystallinity of poly (?-caprolactone), Polym. Int. 49 (2000) 623–626, https://doi.org/10.1002/1097-0126(200006)49:6<623::AID-PI435>3.0.CO;2-8.
[53] N. Romano, C. Araujo-Andrade, J. Lecot, P. Mobili, A. Gómez-Zavaglia, Infrared spectroscopy as an alternative methodology to evaluate the effect of structural features on the physical-chemical properties of inulins, Food Res. Int. 109 (2018) 223–231, https://doi.org/10.1016/j.foodres.2018.04.032.
[54] J.A. Ledermann, Y. Drew, R.S. Kristeleit, Homologous recombination deficiency and ovarian cancer, Eur. J. Cancer 60 (2016) 49–58, https://doi.org/10.1016/j.ejca.2016.03.005.
[55] E. Kokori, G. Olatunji, R. Komolafe, I.C. Abraham, B. Ukoaka, O. Samuel, A. Ayodeji, I. Ogunbowale, C. Ezenwoba, N. Aderinto, Mirvetuximab soravtansine: a breakthrough in targeted therapy for platinum-resistant ovarian cancer, Medicine 103 (2024) e38132, https://doi.org/10.1097/MD.0000000000038132.
[56] X.Z. Zhou, K.P. Lu, The isomerase PIN1 controls numerous cancer-driving pathways and is a unique drug target, Nat. Rev. Cancer 16 (2016) 463–478, https://doi.org/10.1038/nrc.2016.49.
[57] T. Polonio-Vallon, D. KrÃ¼ger, T.G. Hofmann, ShaPINg cell fate upon DNA damage: role of Pin1 isomerase in DNA damage-induced cell death and repair, Front. Oncol. 4 (2014), https://doi.org/10.3389/fonc.2014.00148.
[58] K. Koikawa, S. Kibe, F. Suizu, N. Sekino, N. Kim, T.D. Manz, B.J. Pinch, D. Akshinthala, A. Verma, G. Gaglia, Y. Nezu, S. Ke, C. Qiu, K. Ohuchida, Y. Oda, T. H. Lee, B. Wegiel, J.G. Clohessy, N. London, S. Santagata, G.M. Wulf, M. Hidalgo, S. K. Muthuswamy, M. Nakamura, N.S. Gray, X.Z. Zhou, K.P. Lu, Targeting Pin1 renders pancreatic cancer eradicable by synergizing with immunochemotherapy, Cell 184 (2021) 4753–4771.e27, https://doi.org/10.1016/j.cell.2021.07.020.
[59] W. Wu, X. Xue, Y. Chen, N. Zheng, J. Wang, Targeting prolyl isomerase Pin1 as a promising strategy to overcome resistance to cancer therapies, Pharmacol. Res. 184 (2022) 106456, https://doi.org/10.1016/j.phrs.2022.106456.
[60] M. Zheng, H. Xu, X.-H. Liao, C. Peng Chen, A. Li Zhang, W. Lu, L. Wang, D. Yang, J. Wang, H. Liu, X. Zhen Zhou, K. Ping Lu, Inhibition of the prolyl isomerase Pin1 enhances the ability of sorafenib to induce cell death and inhibit tumor growth in hepatocellular carcinoma, Oncotarget 8 (2017) 29771–29784, https://doi.org/10.18632/oncotarget.15967.
[61] S. Gholamzadeh Khoei, M. Saidijam, R. Amini, A. Jalali, R. Najafi, Impact of PIN1 inhibition on tumor progression and chemotherapy sensitivity in colorectal cancer, J. Gastrointest. Cancer 53 (2022) 299–310, https://doi.org/10.1007/s12029-021-00600-6.
[62] Z.-Z. Zhang, W.-X. Yu, M. Zheng, X.-H. Liao, J.-C. Wang, D.-Y. Yang, W.-X. Lu, L. Wang, S. Zhang, H.-K. Liu, X.Z. Zhou, K.P. Lu, PIN1 inhibition sensitizes chemotherapy in gastric cancer cells by targeting stem cell–like traits and multiple biomarkers, Mol. Cancer Therapeut. 19 (2020) 906–919, https://doi.org/10.1158/1535-7163.MCT-19-0656.
[63] C. Chen, Q. Li, L. Xing, M. Zhou, C. Luo, S. Li, L. Li, Y. Huang, Co-delivery of mitochondrial targeted lonidamine and PIN1 inhibitor ATRA by nanoparticulate systems for synergistic metastasis suppression, Nano Res. 15 (2022) 3376–3386, https://doi.org/10.1007/s12274-021-3923-9.
[64] Y. Liu, F. Yu, S. Dai, T. Meng, Y. Zhu, G. Qiu, L. Wen, X. Zhou, H. Yuan, F. Hu, All-trans retinoic acid and doxorubicin delivery by folic acid modified polymeric micelles for the modulation of Pin1-Mediated DOX-induced breast cancer stemness and metastasis, Mol. Pharm. 18 (2021) 3966–3978, https://doi.org/10.1021/acs.molpharmaceut.1c00220.